Quasi-Homojunction Organic Nonfullerene Photovoltaics Featuring Fundamentals Distinct from Bulk Heterojunctions

Yifan Wang, Michael B. Price,* Raja Sekhar Bobba, Heng Lu, Jingwei Xue, Yilin Wang, Mengyang Li, Aleksandra Ilina, Paul A. Hume, Boyu Jia, Tengfei Li, Yuchen Zhang, Nathaniel J. L. K. Davis, Zheng Tang, Wei Ma, Quinn Qiao, Justin M. Hodgkiss, and Xiaowei Zhan*

In contrast to classical bulk heterojunction (BHJ) in organic solar cells (OSCs), the quasi-homojunction (QHJ) with extremely low donor content (≤10 wt.%) is unusual and generally yields much lower device efficiency. Here, representative polymer donors and nonfullerene acceptors are selected to fabricate QHJ OSCs, and a complete picture for the operation mechanisms of high-efficiency QHJ devices is illustrated. PTB7-Th:Y6 QHJ devices at donor:acceptor (D:A) ratios of 1:8 or 1:20 can achieve 95% or 64% of the efficiency obtained from its BHJ counterpart at the optimal D:A ratio of 1:1.2, respectively, whereas QHJ devices with other donors or acceptors suffer from rapid roll-off of efficiency when the donors are diluted. Through device physics and photophysics analyses, it is observed that a large portion of free charges can be intrinsically generated in the neat Y6 domains rather than at the D/A interface. Y6 also serves as an ambipolar transport channel, so that hole transport as also mainly through Y6 phase. The key role of PTB7-Th is primarily to reduce charge recombination, likely assisted by enhancing quadrupolar fields within Y6 itself, rather than the previously thought principal roles of light absorption, exciton splitting, and hole transport.

1. Introduction

Organic solar cells (OSCs) are a promising next-generation photovoltaic technology since they own some advantages such as printing fabrication, light weight, flexibility, low toxicity, and short energy payback time. The fused-ring electron acceptors (FREAs) pioneered by the Zhan group have broken through the bottleneck of fullerene acceptors,[1–3] and OSCs have achieved revolutionary breakthrough recently.[1–6] To date, power conversion efficiencies (PCEs) of FREA-based OSCs have reached 18–19%.[7–10] Among the diverse FREAs, Y6 (chemical structure shown in Figure S1, Supporting Information) and its derivatives have been widely studied recently due to their high photovoltaic performance.[11–14] Since most organic semiconductors have low dielectric constants ($\varepsilon \approx$ 3–4),[15] Frenkel excitons with high binding energies (E_B) rather than free charges are generated intrinsically upon photoexcitation. Donor (D)/acceptor (A) interfaces that can provide a driving force for exciton dissociation are essential.[16,17] According to the general consensus developed in fullerene-based OSCs, a bulk heterojunction (BHJ) with D/A phase separation size of around 10–20 nm was the optimal morphology for efficient exciton dissociation and charge transport.[18] Accordingly, most high-efficiency optimized OSCs have

Y. Wang
College of Materials Science and Engineering
Qingdao University
Qingdao 266071, P. R. China

Y. Wang, H. Lu, B. Jia, T. Li, X. Zhan
Key Laboratory of Polymer Chemistry and Physics of Ministry of Education
School of Materials Science and Engineering
Peking University
Beijing 100871, P. R. China
E-mail: xwzhan@pku.edu.cn

M. B. Price, A. Ilina, P. A. Hume, N. J. L. K. Davis, J. M. Hodgkiss
MacDiarmid Institute for Advanced Materials and Nanotechnology
School of Chemical and Physical Sciences
Victoria University of Wellington
Wellington 6010, New Zealand
E-mail: michael.price@vuw.ac.nz

The ORCID identification number(s) for the author(s) of this article can be found under https://doi.org/10.1002/adma.202206717.
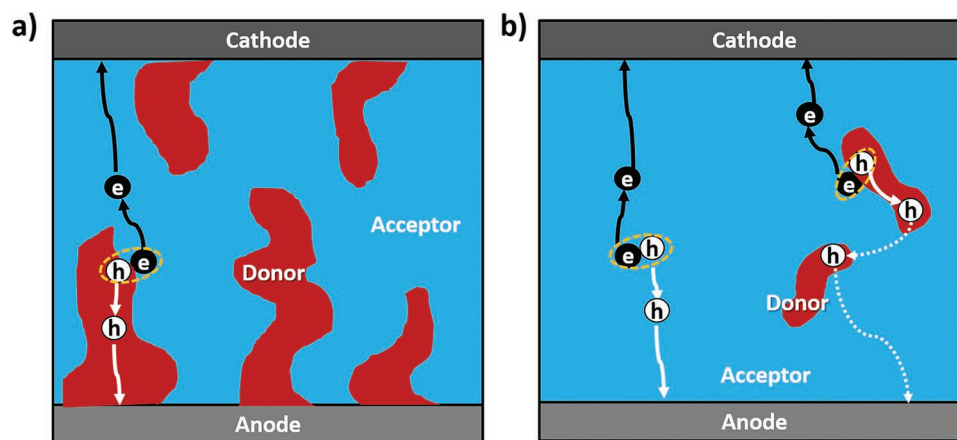
R. S. Bobba, Y. Zhang, Q. Qiao
Department of Mechanical and Aerospace Engineering
Syracuse University
Syracuse, NY 13244, USA

J. Xue, Y. Wang, W. Ma
State Key Laboratory for Mechanical Behavior of Materials
Xi'an Jiaotong University
Xi'an 710049, P. R. China

M. Li, Z. Tang
Center for Advanced Low-Dimension Materials
State Key Laboratory for Modification of Chemical Fibers and Polymer Materials
College of Materials Science and Engineering
Donghua University
Shanghai 201620, P. R. China

**ADVANCED
SCIENCE NEWS**
www.advancedsciencenews.com

**ADVANCED
MATERIALS**
www.advmat.de

Figure 1. a,b) Schemes of operation mechanisms of BHJ (a) and QHJ (b) devices.

approximately equal donor and acceptor concentrations,[19] even with the advent of FREA materials with substantially longer exciton-diffusion lengths.[20] Diluting the donor or acceptor will lead to reduced D/A interface, which would cause insufficient exciton dissociation, unbalanced charge transport, and increased charge recombination.[21] However, the morphology susceptibility of the BHJ architecture may cause processing complexity, inherent energy loss, and morphology instability, which all limit device performance and reproducibility.

In contrast to BHJ, quasi-homojunction (QHJ) with extremely low donor contents (≤10 wt.%) embedded in an acceptor matrix is unusual. QHJ OSCs were first reported by Tang and co-workers in 2011.[22] Interestingly, it was found that efficient charge transport and collection can still be realized in QHJ OSCs,[23] yet the debate still remains about how holes are transported to the electrodes. Some studies revealed hole transport through long-range tunneling from donor to donor molecules even over long distances.[24,25] However, other studies claimed that the fullerene itself could act as an ambipolar semiconductor for both electron and hole-transporting channels.[26,27] Previous studies of QHJ OSCs have mostly focused on charge transport rather than exciton dissociation mechanisms in fullerene-based OSCs. In these systems, it is still universally acknowledged that excitons are dissociated at D/A interfaces in QHJ devices.

As the acceptor is the main light absorber in QHJs, FREA-based devices have much greater potential due to their high light absorption coefficients, particularly in the visible and near-infrared spectral regions, along with substantially different intrinsic photophysics compared with fullerenes.[1] However, studies of FREA-based QHJ devices are still rare. Recently, Yao et al. reported an impressive PCE of over 10% for PM6:Y6 solar cells with only 10 wt.% PM6.[28] This study interpreted hole transport through the dispersed polymer donor, as reasonable mobility was observed for a 10 wt.% PM6 dispersed in the insulating polystyrene matrix. However, compared with the PCEs of ≈16% in optimized PM6:Y6 solar cells, the PCEs of the QHJ devices still dropped considerably.

Recent studies found that Y6 has high ambipolar mobilities, in favor of both electron and hole transport.[29,30] Crucially, Price et al.[31] observed that neat films of Y6 can intrinsically generate

free charge carriers without the help of a D/A interface, through intensity-dependent spectroscopic measurements. However, single-component Y6 devices showed extremely low efficiency due to severe bimolecular and trap-assisted carrier recombination. Karuthedath et al.[32] found that band bending induced by quadrupolar fields at interfaces of donor and acceptor materials can exert considerable effects on the energetics of donor/acceptor HOMO/LUMO levels. Price et al.[31] discussed how this finding could be used to enhance device efficiency in a single material that intrinsically generates charges, by energetically funneling holes away from electrons within Y6 itself. These findings raise questions over whether it is possible to realize high efficiency of QHJ devices by combining intrinsic free charge generation and the ambipolar charge-transport properties of Y6.

In this paper, we systematically studied QHJ OSCs based on different polymer donors and FREA acceptors. We found that the PCEs of PTB7-Th:Y6-based OSCs at D:A ratios of 1:8 or 1:20 can retain 95% or 64% of the champion PCE at the optimized D:A ratio of 1:1.2, respectively. Intriguingly, devices with other donors or FREAs suffer from a drastic decrease in PCE when the donors are diluted. Based on ultrafast transient absorption (TA), current-sensing atomic force microscopy (C-AFM), and morphology characterization, we present a full picture illustrating the operation mechanisms of the high-efficiency QHJ solar cells (**Figure 1**). In the classical BHJ, excitons dissociate at the D/A interface, and the generated electrons/holes transport through the acceptor/donor phases until they are collected by the electrodes. In contrast, in a PTB7-Th:Y6-based QHJ, we observed that a large proportion of free charges are intrinsically generated in neat Y6 phase, rather than at the D/A interface. The hole transport follows two primary mechanisms: holes can tunnel from donor to donor, and/or holes can be transported through the Y6 phase. The latter mechanism becomes more dominant when only small quantities of donor are present, and a purer Y6 phase benefits from less trap-assisted recombination. The primary role of the tiny amount of PTB7-Th is then to prevent charge recombination, likely aided by enhancing quadrupolar fields within the Y6 itself, rather than its standard roles of light absorption, exciton splitting, and hole transport.

**ADVANCED
SCIENCE NEWS**

www.advancedsciencenews.com

**ADVANCED
MATERIALS**

www.advmat.de
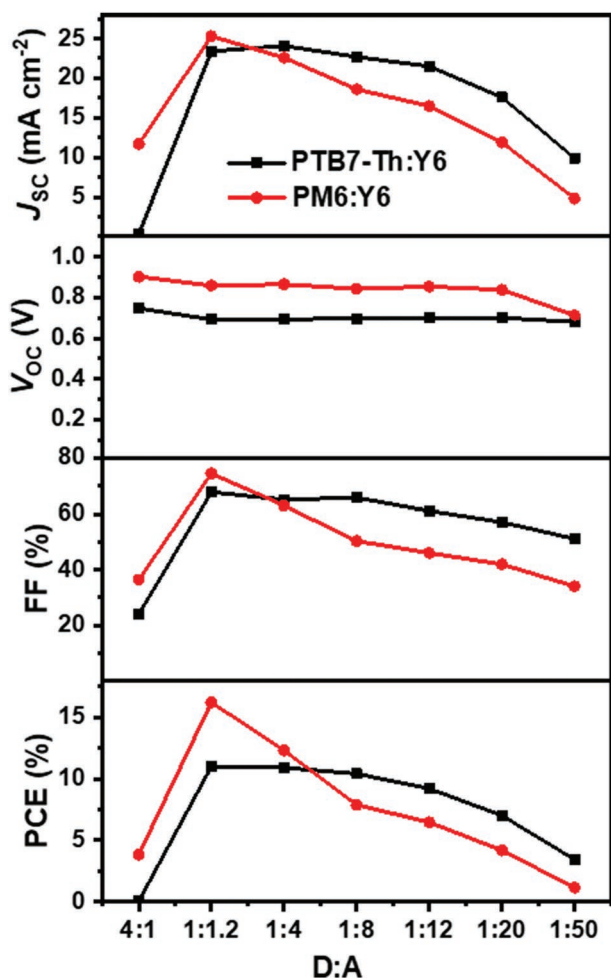
Figure 2. Variation of device performance based on PTB7-Th:Y6 and PM6:Y6 with different D:A ratios.

2. Results and Discussion

2.1. Photovoltaic Performance

First, we investigate the effects of different D:A ratios on device performance based on PTB7-Th:Y6 and PM6:Y6 (molecular structures see Figure S1, Supporting Information) with a structure of ITO/PEDOT:PSS/D:A/PNDIT-F3N/Ag. **Figure 2** shows the variation trends of open-circuit voltage (V_{OC}), short-circuit current density (J_{SC}), fill factor (FF), and PCE with different D:A ratios under AM 1.5G, 100 mW cm^{-2} illumination (corresponding detailed data can be seen in Figures S2a, b and Tables S1 and S2, Supporting Information). With increasing D:A ratio from 1:1.2 to 4:1, the J_{SC}, FF, and PCE of both PTB7-Th:Y6 and PM6:Y6 based devices dramatically decrease, and device performance is highly sensitive to donor concentration. In the diluted donor regime with the D:A ratio changing from 1:1.2 to 1:50, the donor content shows a much smaller influence on device performance compared with the concentrated donor regime. For PTB7-Th:Y6 devices, the PCE only slightly decreases from 11.0% to 10.4% when the D:A ratio significantly decreases from 1:1.2 to 1:8. Even when the PTB7-Th amount is

extremely small, with a D:A ratio of 1:12, 1:20 or 1:50, the PCE still maintains 84%, 64% or 33% of the champion PCE at the optimized D:A ratio of 1:1.2, with losses mainly due to reduced J_{SC} and slightly decreased FF. However, for PM6:Y6 devices, the PCE undergoes a faster decline to 26% and 7.2% of the best PCE at a D:A ratio of 1:20 and 1:50, indicating that the PM6:Y6 device is much more sensitive to the donor loading than the PTB7-Th:Y6 device.

We conducted the thermal stability test for PTB7-Th:Y6 devices with D:A ratios of 1:1.2 and 1:20 at 85 °C in nitrogen atmosphere (Figure S3, Supporting Information). The PCE of PTB7-Th:Y6 (1:1.2) gradually dropped to 50% of its original value after 188.4 h thermal treatment. Surprisingly, the PCE of the QHJ device with a D:A ratio of 1:20 increased to 120% of its original value under thermal treatment for 6 h, and then gradually decreased to 85.8% of its original value after 188.4 h thermal treatment in total. The first few hours of thermal treatment may be equivalent to thermal annealing, which would help to form a better morphology of the active layer, leading to PCE enhancement. The much better thermal stability indicates the improved morphology robustness of the QHJ films.

Then, we compared the device performance of different combinations of donors and acceptors at a D:A ratio of 1:20, including different donors paired with the same acceptor Y6 and different acceptors paired with the same donor PTB7-Th (Table S3, Supporting Information). The results show that the PTB7-Th:Y6 QHJ devices outperform others. We also test single-component OSCs based on PTB7-Th, PM6, or Y6 (Table S4, Supporting Information). However, all the PCEs are extremely low (0.05%–0.1%), indicating a tiny loading of donors plays a key role in QHJ OSCs.

External quantum efficiency (EQE) spectra of PTB7-Th:Y6 and PM6:Y6 based devices were characterized to shed light on the J_{SC} variation with different D:A ratios (**Figure 3**a,b). All the J_{SC} values calculated from EQE measurements match well with measured J_{SC} values (Tables S1 and S2, Supporting Information). We note that for PTB7-Th:Y6 devices, when Y6 loading increases more than a 1:1.2 D:A ratio, a slight redshift of EQE spectra is observed, perhaps due to increased molecular ordering of Y6, whereas PM6:Y6 devices do not show such redshift. It is also worth noting that when the donor content decreases, both EQE contributions of donors and acceptors decrease at a similar rate, which is the opposite of the typically expected behavior—donor contributions decrease much faster than acceptor contributions. This suggests electrons and holes maintain relatively balanced transport even at extremely small donor contents. The absorption spectra of blend films with different D:A ratios were also measured (Figure 3c,d). The absorption spectra of PTB7-Th:Y6 redshift when the D:A ratio is smaller than 1:1.2, consistent with the EQE trends. When the D:A ratio decreases, both absorption of PTB7-Th and PM6 decrease considerably, which is different from the EQE trend, suggesting that light absorption is not the only factor responsible for different device performance at different D:A ratios.

2.2. Device Physics

Having identified anomalously high PCEs in PTB7-Th:Y6 QHJ devices, we investigate/compare in detail the electronic and
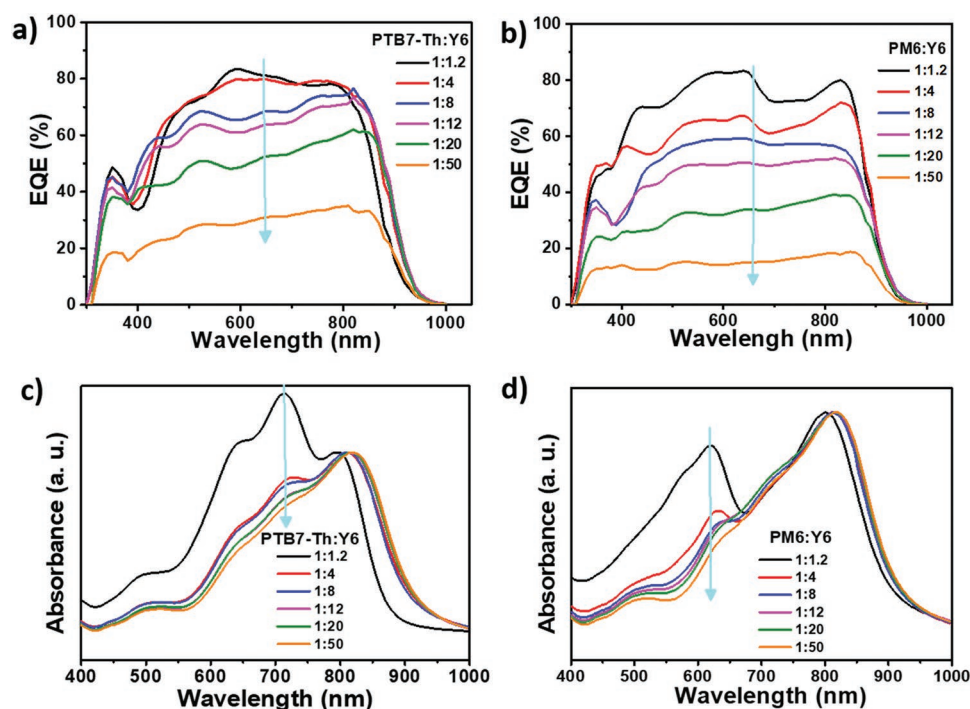
Figure 3. a,b) EQE spectra of PTB7-Th:Y6 (a) and PM6:Y6 (b) at different D:A ratios. c,d) Absorption spectra of PTB7-Th:Y6 (c) and PM6:Y6 (d) at different D:A ratios.

photophysical processes across four different representative devices based on PTB7-Th:Y6 and PM6:Y6 with D:A ratios of 1:1.2 and 1:20. We seek to answer key questions such as: Why is PTB7-Th so much better than other donors? What are the timescales of exciton and charge recombination? And how does charge transport proceed once charges and excitons have traveled through the acceptor and reached a donor site?

First, we study charge recombination behaviors in the devices by analyzing V_{OC} and J_{SC} dependence on light intensity (P_{light}) (Figure S4, Supporting Information).[33,34] The slope of $V_{OC} \propto \ln(P_{light})$ is fitted to be 1.19 kT/e (where k is the Boltzmann constant, T is the Kelvin temperature, and e is the elementary charge) and 1.22 kT/e for PTB7-Th:Y6 based devices with D:A ratios of 1:1.2 and 1:20, respectively. These values suggest that bimolecular recombination dominates in both devices. The slope of $V_{OC} \propto \ln(P_{light})$ increases from 1.09 kT/e to 1.46 kT/e for PM6:Y6-based devices when the D:A ratio decreases from 1:1.2 to 1:20, indicating monomolecular recombination notably increases at an extremely low PM6 loading. At very low light intensities (e.g., 0.9 mW cm^{-2}), PM6:Y6 QHJ devices show a drastic decrease of V_{OC}, heavily deviating from the linear relation of V_{OC} versus $\ln(P_{light})$, which indicates massive recombination, likely caused by the unsaturated hole traps reported by Yao et al.[28] and Price et al.[31] J_{SC} and P_{light} follow the relationship of $J_{SC} \propto P_{light}^{\alpha}$, where α describes the degree of bimolecular recombination ($\alpha = 1$ manifests no bimolecular recombination). The α values decrease from 0.896 to 0.841 for PTB7-Th:Y6 devices and from 0.931 to 0.844 for PM6:Y6 devices with the D:A ratio decreasing from 1:1.2 to 1:20, indicating that the degree of bimolecular recombination increases with decreasing donor loading for both PTB7-Th and PM6-based devices.

Charge-transport behaviors were initially investigated by measuring charge mobilities using the space-charge-limited current method (Figures S5 and S6, Table S5, Supporting Information).[35] We first measured the hole mobilities of PM6 and PTB7-Th and hole and electron mobilites of Y6. Y6 exhibited high ambipolar mobilities with a hole mobility (μ_h) of 9.30×10^{-4} cm^2 V^{-1} s^{-1} and electron mobility (μ_e) of 3.04×10^{-4} cm^2 V^{-1} s^{-1}. We then measured the charge mobility of the four devices based on PTB7-Th:Y6 and PM6:Y6 with D:A ratios of 1:1.2 and 1:20. Compared with the PTB7-Th:Y6 (1:1.2) samples, PTB7-Th:Y6 QHJ samples (D:A = 1:20) show similar μ_e ($1.43/1.44 \times 10^{-3}$ cm^2 V^{-1} s^{-1}) and decreased μ_h (from 6.49×10^{-4} to 1.43×10^{-4} cm^2 V^{-1} s^{-1}). PM6:Y6 QHJ samples show a marked decrease of μ_e (from 1.56×10^{-3} to 1.72×10^{-5} cm^2 V^{-1} s^{-1}) and a marked decrease of μ_h (from 7.03×10^{-4} to 3.4×10^{-6} cm^2 V^{-1} s^{-1}). The low charge mobilities of PM6:Y6 QHJ result in poor charge-transport properties.

We then used C-AFM to map the charge-carrier dynamics, which could provide a direct view of the local nanoscale electrical properties.[36,37] Figure S7a, b, Supporting Information, and **Figure 4**a, b show 1 μm × 1 μm C-AFM images of PTB7-Th:Y6 (1:1.2), PM6:Y6 (1:1.2), PTB7-Th:Y6 (1:20) and PM6:Y6 (1:20) samples, respectively. The average currents for PTB7-Th:Y6 (1:1.2), PTB7-Th:Y6 (1:20), PM6:Y6 (1:1.2), and PM6:Y6 (1:20) samples are 73, 41, 61, and 35 pA, respectively. In the C-AFM images, the more conductive region can be classified as the electron-rich domain, whereas the less conductive region represents the electron-poor domain.[36,37] Our C-AFM is set to selectively detect the electron current from the active layer on a ZnO substrate. Generally, an electron-rich region is equal to an acceptor-rich region, but in our case, we see interesting

**ADVANCED
SCIENCE NEWS**

www.advancedsciencenews.com

**ADVANCED
MATERIALS**

www.advmat.de
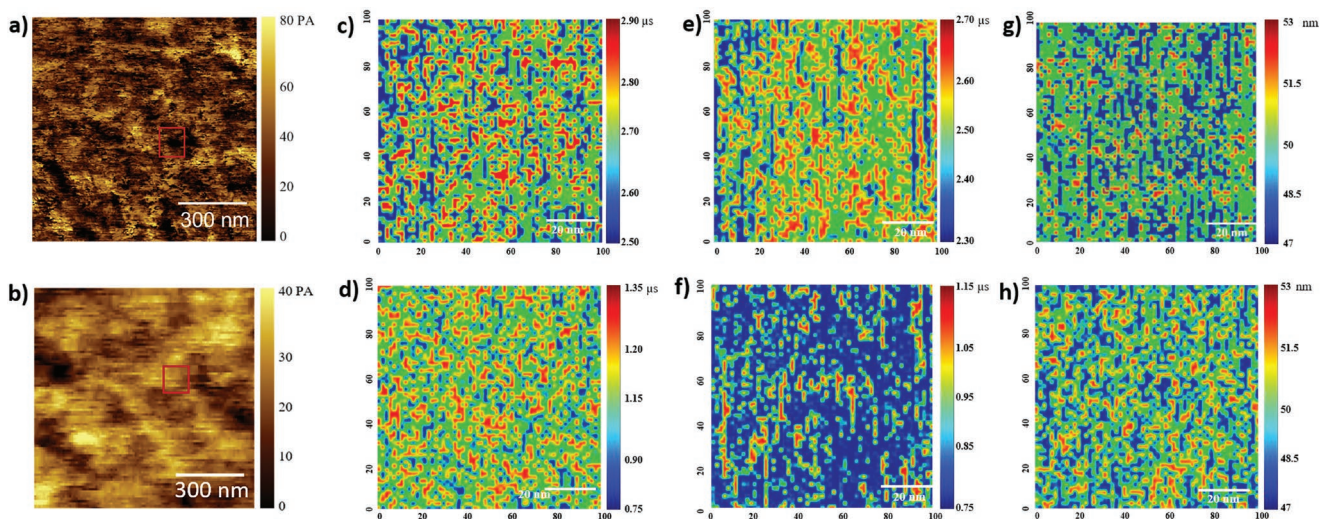
Figure 4. a,b) C-AFM images of PTB7-Th:Y6 (1:20) (a) and PM6:Y6 (1:20) (b) samples. c,d) Nanoscale mapping of τ_r for PTB7-Th:Y6 (1:20) (c) and PM6:Y6 (1:20) (d) samples. e,f) Nanoscale mapping of τ_t for PTB7-Th:Y6 (1:20) (e) and PM6:Y6 (1:20) (f) samples. g,h) Nanoscale mapping of L_D for PTB7-Th:Y6 (1:20) (g) and PM6:Y6 (1:20) (h) samples. The mappings were all from 100 nm × 100 nm red square regions in C-AFM images.

phenomena. For the PM6:Y6 QHJ sample, the bright region occupies the majority, which is reasonable because of such a predominant acceptor content. While for the PTB7-Th:Y6 QHJ sample, the bright and dark regions are almost evenly distributed. If Y6 only undertakes electron transport in a PTB7-Th:Y6 QHJ, the C-AFM image should be bright for the most part. Therefore, this uncommon C-AFM image gives an initial indication that Y6 serves as an ambipolar charge-transport channel in PTB7-Th:Y6 QHJ OSCs.

A 100 nm × 100 nm area is shown by the red square on the C-AFM images, which were used for mapping nanoscale charge-carrier dynamics such as charge-carrier lifetime (τ_r), charge-transport time (τ_t), and charge-diffusion length (L_D), through local transient photovoltage and transient photocurrent measurements. The charge-dynamics data are summarized in Table S6, Supporting Information. Figure S7c, d, Supporting Information, presents the nanoscale τ_r mapping of PTB7-Th:Y6 and PM6:Y6 BHJ samples at D:A = 1:1.2. To compare charge-carrier dynamics between the samples, both donor-rich and acceptor-rich regions are labeled by white dashed lines for the BHJ samples. Due to the extremely high ratio of Y6 in QHJ samples, there are no identifiable donor-rich regions. Figure 4c,d shows the nanoscale τ_r mapping of PTB7-Th:Y6 and PM6:Y6 QHJ samples at D:A = 1:20. The QHJ samples show reduced τ_r compared with the BHJ samples, which is reasonable because of more charge recombination caused by larger acceptor domains. While the PTB7-Th:Y6 QHJ exhibits a much higher mean τ_r of 2.67 μs than that of the PM6:Y6 QHJ (1.15 μs), suggesting that charge recombination in the PM6:Y6 QHJ samples occurs much faster than the PTB7-Th:Y6 QHJ samples.

Figure S7e, f, Supporting Information, and Figure 4e,f present the nanoscale charge-transport time, τ_t, mapping of the four samples. In Table S5, Supporting Information, the mean τ_t in PTB7-Th:Y6 (1:1.2), PTB7-Th:Y6 (1:20), PM6:Y6 (1:1.2), and PM6:Y6 (1:20) samples are 5.17, 2.43, 4.55, and 0.95 μs, respectively. As Y6 content increases with the D:A ratio from 1:1.2

to 1:20, the electron-transport path along the acceptor domain increases, leading to a much faster electron-transport time. Though the transport time for the PTB7-Th:Y6 QHJ is slower than that for the PM6:Y6 QHJ, the recombination time is also much longer, which explains the overall superior device performance of the PTB7-Th:Y6 QHJ. It is noticed that τ_r is larger than τ_t in both QHJ devices, indicating that charges can be collected before they recombine.

The nanoscale L_D mapping of the four samples is shown in Figure S7g, h, Supporting Information, and Figure 4g,h. The mean L_D in PTB7-Th:Y6 (1:1.2), PTB7-Th:Y6 (1:20), PM6:Y6 (1:1.2), and PM6:Y6 (1:20) samples are 67.0, 50.6, 68.0, and 49.5 nm respectively. As the donor content decreases, the L_D decreases, which may be caused by increased bimolecular recombination. As the film thickness of QHJ devices is ca. 70 nm, most generated electrons still can reach the electrodes. The L_D of PTB7-Th:Y6 QHJ is a bit larger than that of PM6:Y6 QHJ, which is consistent with the device performance.

There are two different trends for V_{OC} variation between PTB7-Th:Y6 and PM6:Y6 devices; V_{OC} increases for PTB7-Th:Y6 devices while V_{OC} decreases for PM6:Y6 devices when the D:A ratio changes from 1:1.2 to 1:20. The different trends in V_{OC} variation can be ascribed to different energy losses. Thus, we performed highly sensitive EQE (sEQE), electroluminescence (EL), and EQE_{EL} measurements to determine energy losses of the devices.[38,39] The E_g values for the blend films were determined from the crossing point of the photoluminescence and absorption spectra of the pure Y6 film by method from the literature.[40] **Table 1** shows the calculated energy loss parameters of the devices. More specifically, we first determined the radiative recombination limit for the device V_{OC} ($V_{OC,rad}$), from the sEQE and EL measurements (Figure S8, Supporting Information), using the method described in the literature.[41] $V_{OC,rad}$ is found to be 1.016 and 1.023 V for PTB7-Th:Y6 devices with D:A ratios of 1:1.2 and 1:20, respectively. Nonradiative recombination voltage loss (ΔV_{nr}), calculated as difference between $V_{OC,rad}$ and measured V_{OC}, was then determined, which were

**ADVANCED
SCIENCE NEWS**

www.advancedsciencenews.com

**ADVANCED
MATERIALS**

www.advmat.de

Table 1. Energy loss parameters of blended films at different D:A ratios.

Sample	V_{OC} [V]	E_{CT} [eV]	EQE_{EL}	E_g [eV]	$V_{OC,rad}$ [V]	ΔV_{nr}[a] [V]	ΔV_{nr}[b] [V]	ΔV_r [V]
PTB7-Th:Y6 = 1:1.2	0.692	1.30	1.02×10^{-6}	1.40	1.016	0.324	0.345	0.384
PTB7-Th:Y6 = 1:20	0.700	1.33	1.16×10^{-6}	1.40	1.023	0.323	0.341	0.377
PM6:Y6 = 1:1.2	0.859	1.35	2.69×10^{-4}	1.40	1.051	0.192	0.205	0.349
PM6:Y6 = 1:20	0.838	1.33	2.37×10^{-4}	1.40	1.029	0.191	0.209	0.371

[a]Calculated from $V_{OC,rad}$; [b]Calculated from EQE_{EL}.

0.324 and 0.323 V for the PTB7-Th:Y6 devices with D:A ratios of 1:1.2 and 1:20, respectively. We also determined ΔV_{nr} using the equation:

$$\Delta V_{nr} = \frac{kT}{q}\ln\left(\frac{1}{EQE_{EL}}\right) \tag{1}$$

where EQE_{EL} is the measured EL EQE of the solar cell (Figure S9, Supporting Information). The ΔV_{nr} determined by the EQE_{EL} measurements were 0.345 and 0.341 V for the PTB7-Th:Y6 devices with D:A ratios of 1:1.2 and 1:20, respectively. Since the values for ΔV_{nr} are found to be similar for the devices with D:A ratios of 1:1.2 and 1:20, we conclude that the difference in V_{OC} of the devices with different D:A ratios is not due to different non-radiative recombination voltage losses. Then, we calculated the radiative recombination voltage losses (ΔV_r), defined as the difference between E_g/q and $V_{OC,rad}$, and we found that ΔV_r were 0.384 and 0.377 eV for the PTB7-Th:Y6 devices with D:A ratios of 1:1.2 and 1:20, respectively. Thus, the main reason for the different V_{OC} is ascribed to the different radiative recombination voltage loss. We also performed similar analyses for the devices based on PM6:Y6 with different D:A ratios. We found that ΔV_{nr} were similar, about 0.19–0.2 V, for the PM6:Y6 devices with different D:A ratios. However, ΔV_r of the PM6:Y6 device with a D:A ratio of 1:20 was higher than that with a D:A ratio of 1:1.2 (0.371 vs 0.349 V). Therefore, V_{OC} is reduced by reducing the D:A ratio for the PM6:Y6 device, unlike that observed for the PTB7-Th:Y6 devices.

2.3. Photophysics

To gain a complete picture of both exciton and charge dynamics on a picosecond scale, compared to the microsecond time-scale of the above measurements, we performed ultrafast TA on a series of thin films of Y6 with differing donor PTB7-Th content, and used a genetic algorithm to extract dynamics of different species.[31,42] Due to the spectrally different polaron photoinduced absorption of the PTB7-Th, we are able to spectrally resolve the donor hole polaron, the acceptor charge-transfer state/electron, and the acceptor exciton. The spectral masks used for our analysis in the near-infrared spectral region are shown in Figure S10, Supporting Information. Other studies[28,43] have looked at hole transfer based on the bleach of the polymer donor, in a region where the acceptor kinetics are approximately zero. This, however, relies on the assumption that electroabsorption[42] does not alter the spectra when the two materials are present as a blend. Hence, we have taken a more in-depth approach to rule out such effects, and also differentiate

the kinetics of the relevant species in the system (donor hole polaron, acceptor exciton, and acceptor electron polaron).

The kinetics of these species for four different PTB7-Th:Y6 ratios are shown in **Figure 5**. As expected, the kinetics of the PTB7-Th hole polaron (orange lines) show an increasing fraction of prompt hole generation, and faster rise kinetics, as the portion of PTB7-Th in the blend increases. We also see that the Y6 charge/CT species (purple line), and the PTB7-Th hole species show different kinetics, in agreement with Wang et al.[43] and Price et al.[31] However, after ≈500 ps, the Y6 charge and PTB7-Th species appear to show similar decay kinetics, as would be expected.

Interestingly, though one would expect the Y6 exciton (pink lines) to be quenched more rapidly with increasing PTB7-Th content, this is the case only for the very prompt initial kinetic component (within the first 10 ps), as evidenced by a faster apparent rise time and decay within the instrument response time (particularly for the 1:1.2 blend). **Figure 6**a compares the un-normalized exciton kinetics for the different D:A ratios. After the initial faster quench of the exciton for the 1:1.2 blend, the exciton kinetics are in fact delayed compared to the lower donor proportion blends. This could potentially be due to an extra electroabsorption-type feature that matches closely to the exciton spectra appearing at later times as charges are separated. However, an alternative explanation is that there is a significant charge-to-exciton recombination channel, and the separated charges in the different phases can recombine back into excitons in Y6 in measurable quantities. While at first glance this would appear to be an energetically unfavorable process, it is in fact in good agreement with the energy level bending expected in the system based on the proposal by Karuthedath et al.[32] The expected ≈300 meV level shifts of both ionization energy and electron affinity would be sufficient to allow for significant transfer of separated charges back to excitons.

Figure 6b shows the hole kinetics of the PTB7-Th for different D:A ratio films. By looking at the peak value of these hole kinetics (with the option of adding the additional exciton component as well), we can compare to trends seen in the steady-state device EQE measurements. Figure 6c shows the maximum value of the signal from holes in PTB7-Th (plus the remaining exciton portion), normalized to the peak experimental EQE value of 0.8/80% (black triangles), compared to the device EQE values (blue squares). Across the range of D:A ratios, we see that the TA signal from holes in the donor roughly matches the trend for device EQEs. If charge transport and percolation pathways were 100% efficient, then these values from the TA should match or exceed the values from
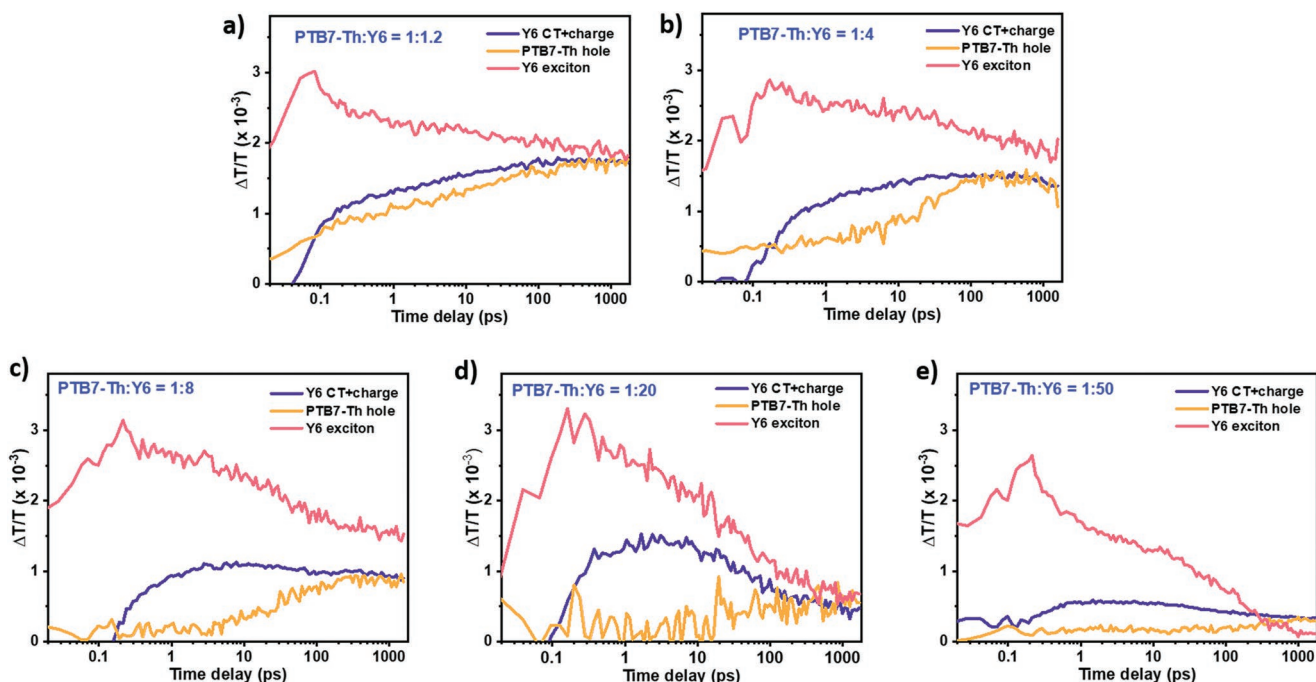
Figure 5. Kinetics of the exciton in Y6 (pink), the charge plus CT populations in Y6 (purple), and the hole population in PTB7-Th (orange), for different D:A ratios extracted from the TA spectra using the genetic algorithm. All films were excited with 800 nm, 150 fs pulses, at ≈5μJ cm^{-2} fluences.

device measurements. In reality, the predicted EQE trend with decreasing PTB7-Th content from TA gives EQEs lower than EQEs in the device results. This is a further indication that recombination due to morphological traps and poor charge transport is small. It shows that at the fluences we have measured, the transient kinetics suffer from some bimolecular recombination before charge separation. This again highlights the importance of reducing bimolecular recombination through charge separation.[31,44]

We can also use the rate of hole transfer to get a rough estimate of the exciton and charge diffusion from Y6 to PTB7-Th, after any prompt transfer has occurred. Figure S11a, Supporting Information, shows exponential fits to the rise of the PTB7-Th hole signal between 10 and 300 ps. The transfer rate, as expected, decreases as PTB7-Th concentration decreases.

We employ a modified Stern–Volmer (S–V)-type analysis to gain more intuition about the photophysics of the Y6 exciton, charge, and CT-state diffusion and subsequent transfer to PTB7-Th after the prompt and coherent processes have occurred. Based on molecular weight and densities of PTB7-Th and Y6,[16,45] we can calculate the predicted chromophore density of PTB7-Th within the Y6 matrix. If these chromophores were dispersed evenly throughout the film, we would have: $k_{rise} = 4\pi RD[Q]$, where $[Q]$ is the chromophore density, R is the exciton or charge quenching radius from Y6 to PTB7-Th, and D is the effective exciton/charge-diffusion constant. Figure S11b, Supporting Information, shows that this relationship very roughly holds, although as expected, the increase in transfer rate tails off as the PTB7-Th density increases due to aggregation of PTB7-Th. Bimolecular recombination of the excitons and charges in Y6 will also cause deviations
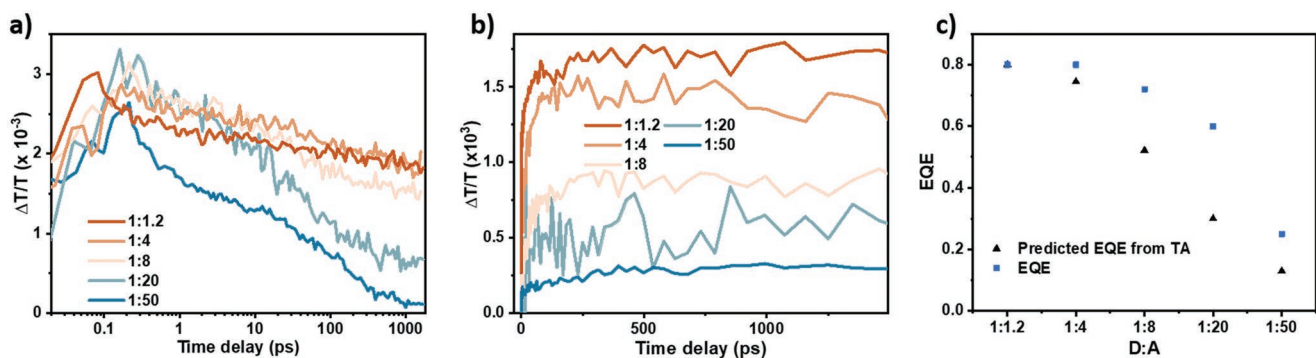
Figure 6. a) Exciton kinetics in Y6, for different D:A ratios, as shown in Figure 5. b) PTB7-Th hole kinetics for given D:A ratios. c) Predicted EQE from the peak of the charge species kinetics in TA (normalized to 0.8), compared to the EQE from device measurements at a wavelength of 800 nm.

from this relationship. If we fit a power law expression to the S–V plot,[46] and extrapolate to zero chromophore density, the effects of PTB7-Th aggregation will also tend to zero, and hence the slope at small PTB7-Th densities should be roughly proportional to the Y6 hybrid exciton–charge diffusion constant. With $R = 1$ nm, we obtain an effective diffusion constant, $D = 0.2 \times 10^{-2}$ cm^2 s^{-1}. As we are selectively looking at the delayed diffusion component, we would expect a lower value than others have obtained previously. Encouragingly though, as would be expected based on our device results, and the results of Price et al.,[31] this diffusion constant is in reasonable agreement with the expected charge diffusivity based on mobility measurements,[47] of $D = 0.13 \times 10^{-2}$ cm^2 s^{-1}. Our value is approximately 20 times smaller than values obtained in the literature[47] for exciton diffusivity by other methods that include prompt plus delayed quenching in a neat Y6 material, or methods that focus on exciton-exciton bimolecular recombination. We note however that effects of bimolecular recombination, aggregation, incomplete exciton/charge quenching (and the charge-exciton back-transfer described above), could potentially artificially lower our diffusion constant value also.

From the above device physics and photophysics studies, we can conclude that across all the time scales—from femtoseconds to milliseconds, the working mechanisms in these high-efficiency QHJ devices based on PTB7-Th:Y6 are working in ways not traditionally expected in standard BHJ OSCs. Before 100 ps, instead of exciton transport within the donor/acceptor followed by charge separation, charges are immediately separated in Y6 itself, as evidenced by the TA measurements. On the nano-microsecond timescale (as evidenced by the transient photovoltage/photocurrent measurements) once charges have diffused to donor sites—rather than the holes hopping exclusively through the donor and electrons transporting through acceptor domains—there is substantial hole transport occurring within Y6 as well.

2.4. Morphology

The above results provide significant clues as to why PTB7-Th:Y6 QHJs outperform PM6:Y6 QHJs, but morphology characterization is needed to better understand how it is that these samples can generate such unexpected photophysics. First, grazing-incidence wide-angle X-ray scattering (GIWAXS) measurements were adopted to provide molecular packing information.[48,49] The 2D GIWAXS patterns and corresponding 1D profiles along out-of-plane (OOP) and in-plane (IP) directions of neat PTB7-Th, PM6, and Y6 films can be found in Figure S12, Supporting Information. The neat Y6 film shows (100) and (001) diffraction peaks in the IP direction and a strong (010) peak in OOP direction, indicating efficient π–π stacking and a preferred face-on orientation. The (001) diffraction peak originates from the backbone ordering due to the end-group π–π stacking, which is beneficial to improve the intermolecular electron transport. The PM6:Y6 and PTB7-Th:Y6 blend films with different ratios display a strong diffraction peak in the OOP direction at $q = 1.75$Å^{-1}, associated with the π–π stacking of Y6 (Figure S13, Supporting Information). It is worth noting that in the IP direction, the scattering peak at $q = 0.420$ Å^{-1} is strongly

increased in the PM6:Y6 (1:20) and PTB7-Th:Y6 (1:20) films, indicative of significant enhancement of backbone ordering of Y6, which would lead to better charge-transport properties. However, there are no visible differences in GIWAXS parameters between the PM6:Y6 (1:20) and PTB7-Th:Y6 (1:20) films. Therefore, the performance difference between the two systems does not originate from molecular packing properties.

The phase separation properties of the films were detected by resonant soft X-ray scattering (RSoXS).[50,51] The high contrast scattering information of these organic materials was obtained at an X-ray energy of 284.8 eV (**Figure 7**, Table S7, Supporting Information). The scattering peaks of PM6:Y6 (1:1.2) and PTB7-Th:Y6 (1:1.2) films are at $q = 0.145$ nm^{-1} and 0.103 nm^{-1}, respectively, from which we calculate that the domain size of PTB7-Th:Y6 (21.7 nm) is smaller than that of PM6:Y6 (30.6 nm) at an optimal D:A ratio. The domain sizes of the QHJ samples are obviously increased compared with the samples with optimal D:A ratios, which are 109 and 103 nm for PTB7-Th:Y6 and PM6:Y6 QHJ, respectively. The large domain size is far beyond the exciton-diffusion length of organic semiconductors (≈10–20 nm), although the exciton-diffusion length of Y6 is larger (ca. 40 nm) according to the previous literature.[47] It means that most excitons would recombine if they can only be dissociated at the D/A interface. However, the QHJ samples, especially devices based on PTB7-Th:Y6, still yield surprisingly high PCE and low charge recombination, again attesting that the D/A interface does not play a key role in exciton dissociation. The relative phase purity of the PTB7-Th:Y6 system is improved from 0.63 to 1 as the D:A ratio changes from 1:1.2 to 1:20, which means that the two phases of donor and acceptor separate with sharp interfaces in the QHJ device. In contrast, the relative phase purity of the PM6:Y6 system decreases a little from 0.67 to 0.64 when the D:A ratio changes from 1:1.2 to 1:20, meaning that the small amount of PM6 is well dispersed in the Y6 phase.

Detailed knowledge of film morphologies, combined with our previous electrical and photophysical measurements, allows us to further address the issue of hole transport in our QHJ devices. There are two primary hole-transport options available. The first option is that holes tunnel exclusively from one donor molecule to another. In this case, the PM6:Y6 system would likely exhibit better performance because the well-dispersed PM6 would reduce the likelihood of large donor-donor distances for hole tunneling to overcome. As the PM6:Y6 QHJ in fact shows inferior hole transport compared with the PTB7-Th:Y6 QHJ, this scenario is not the main hole-transport mechanism (although there is the possibility that the less-dispersed PTB7-Th is arranged in a morphology more favorable to hole-transport, such as through forming nanofibrils—although we see no evidence of this).

The second option is that Y6 serves as an ambipolar transport channel. Y6 plays a carrier-transport role for both electrons and holes, while the donors act as both detrimental traps/recombination centers, or beneficial charge-separation and transport pathways. As PTB7-Th:Y6 QHJs have much purer Y6 phases than PM6:Y6 QHJs, if the holes transport through the Y6, the purer phase and sharper interfaces would suppress charge recombination. The RSOXS measurement thus provides additional evidence of hole transport in Y6 and explains
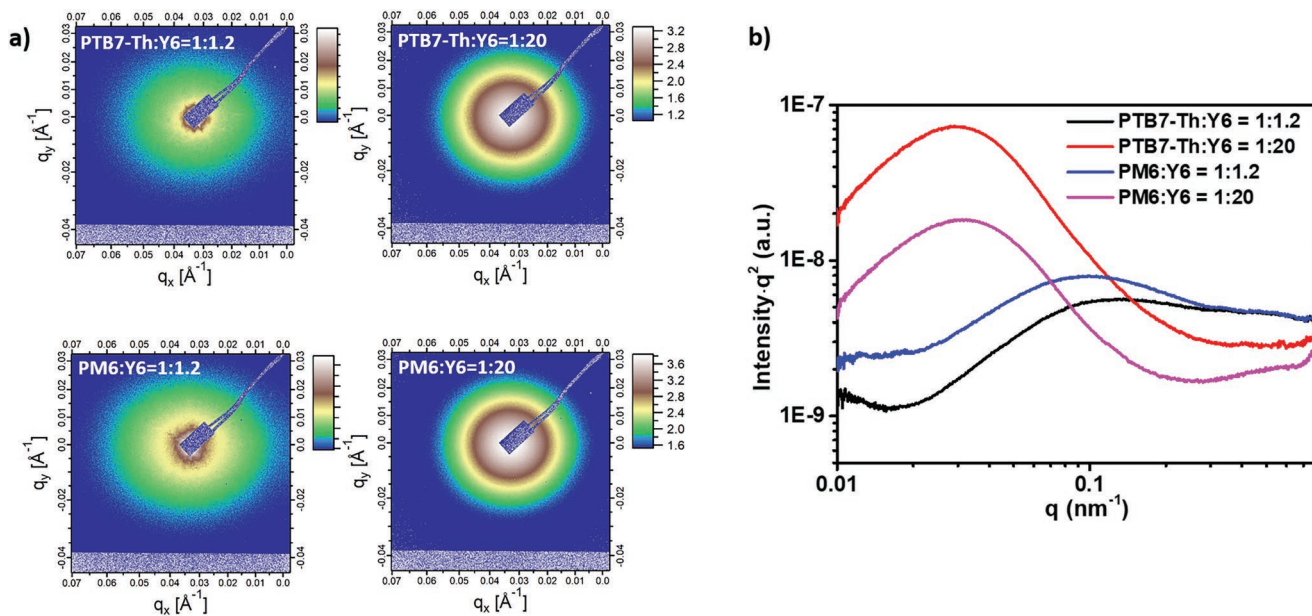
Figure 7. a) 2D RSoXS patterns obtained at an X-ray energy of 284.8 eV and b) RSoXS scattering profiles of blended films at different D:A ratios.

why PTB7-Th:Y6 QHJ outperforms PM6:Y6 QHJ. As hinted at in the TA measurement, interfacial effects such as dipolar interactions,[52] will affect recombination kinetics. Band-bending induced by quadrupolar fields[32] could possibly also enhance charge transport by physically/energetically separating electrons and holes within the Y6 phase itself. Quadrupolar field strengths[53,54] are maximized by highly ordered pure domains and sharp interfaces with minimal donor-acceptor mixing.[32] This may explain why this effect would be more pronounced for the purer domains of the PTB7-Th:Y6 compared to the PM6:Y6.

3. Conclusions

Nonfullerene OSCs based on QHJ with extremely low donor contents were studied by varying donors, acceptors, and D:A ratios. Surprisingly, for PTB7-Th:Y6 devices, at D:A ratios of 1:8 or 1:20, the device efficiencies still retain 95% or 64% of the champion PCE at the optimal D:A ratio of 1:1.2, respectively. QHJ devices with other donors or FREA acceptors suffer from serious roll-off of PCEs when the donors are largely diluted. A large portion of charges can be intrinsically generated in the neat Y6 domains in PTB7-Th:Y6 QHJ devices, rather than at the D/A interface. Y6 also serves as an ambipolar transport channel, so that efficient hole transport is realized despite such a small amount of donors. PTB7-Th:Y6 QHJs outperform PM6:Y6 QHJs, mainly benefitting from the much purer Y6 domains in PTB7-Th:Y6 QHJs, which facilitate charge transport in the Y6 itself, enhance band-bending through quadrupolar fields, and reduce carrier recombination at interfaces. The primary role of the small amount of PTB7-Th is to prevent charge recombination, and enhance quadrupolar fields within the Y6 itself. This is different from the traditional roles of donors which are to absorb light, facilitate exciton dissociation, and transport holes.

We presume that high-efficiency QHJ devices should meet the following requirements: 1) The main component should be high-efficiency FREA materials with wide-range intense visible and near-infrared light absorption, efficient ambipolar charge transport, and capable of spontaneously generating charge carriers without the help of D/A interface. 2) The minor component should be a high-efficiency p-type donor with energy levels matching well with the FREA main component, which could yield a large V_{OC}. 3) The FREA and donor materials should form a morphology with large and pure acceptor domains, which can facilitate charge transport and reduce bimolecular carrier recombination, and enhance band-bending through quadrupolar fields and charge separation even within the FREA domains.

Our work opens a door for new OSC structures beyond the classical bulk heterojunction, where high device efficiency can be realized by improving intrinsic charge generation and reducing charge recombination, rather than only relying on exciton dissociation at D/A interfaces. This new device structure can also be applicable to other applications such as semitransparent OSCs and near-infrared photodetectors.

Supporting Information

Supporting Information is available from the Wiley Online Library or from the author.

Acknowledgements

**ADVANCED
SCIENCE NEWS**

www.advancedsciencenews.com

**ADVANCED
MATERIALS**

www.advmat.de

Conflict of Interest

The authors declare no conflict of interest.

Data Availability Statement

The data that support the findings of this study are available from the corresponding author upon reasonable request.

Keywords

[1] J. Y. Wang, P. Y. Xue, Y. Jiang, Y. Huo, X. W. Zhan, *Nat. Rev. Chem.* **2022**, *6*, 614.

[2] C. Yan, S. Barlow, Z. Wang, H. Yan, A. K. Y. Jen, S. R. Marder, X. W. Zhan, *Nat. Rev. Mater.* **2018**, *3*, 18003.

[3] Y. Z. Lin, J. Y. Wang, Z. G. Zhang, H. T. Bai, Y. F. Li, D. B. Zhu, X. W. Zhan, *Adv. Mater.* **2015**, *27*, 1170.

[4] A. J. Gillett, A. Privitera, R. Dilmurat, A. Karki, D. Qian, A. Pershin, G. Londi, W. K. Myers, J. Lee, J. Yuan, S.-J. Ko, M. K. Riede, F. Gao, G. C. Bazan, A. Rao, T.-Q. Nguyen, D. Beljonne, R. H. Friend, *Nature* **2021**, *597*, 666.

[5] L. Meng, Y. Zhang, X. Wan, C. Li, X. Zhang, Y. Wang, X. Ke, Z. Xiao, L. Ding, R. Xia, H. L. Yip, Y. Cao, Y. S. Chen, *Science* **2018**, *361*, 1094.

[6] P. Cheng, G. Li, X. W. Zhan, Y. Yang, *Nat. Photonics* **2018**, *12*, 131.

[7] C. Li, J. Zhou, J. Song, J. Xu, H. Zhang, X. Zhang, J. Guo, L. Zhu, D. Wei, G. Han, J. Min, Y. Zhang, Z. Xie, Y. Yi, H. Yan, F. Gao, F. Liu, Y. M. Sun, *Nat. Energy* **2021**, *6*, 605.

[8] J. Wang, Z. Zheng, Y. Zu, Y. Wang, X. Liu, S. Zhang, M. Zhang, J. H. Hou, *Adv. Mater.* **2021**, *33*, 2102787.

[9] H. Meng, C. Liao, M. Deng, X. Xu, L. Yu, Q. Peng, *Angew. Chem., Int. Ed.* **2021**, *60*, 22554.

[10] S. Bao, H. Yang, H. Fan, J. Zhang, Z. Wei, C. Cui, Y. F. Li, *Adv. Mater.* **2021**, *33*, 2105301.

[11] J. Yuan, Y. Zhang, L. Zhou, G. Zhang, H.-L. Yip, T.-K. Lau, X. Lu, C. Zhu, H. Peng, P. A. Johnson, M. Leclerc, Y. Cao, J. Ulanski, Y. Li, Y. P. Zou, *Joule* **2019**, *3*, 1140.

[12] Y. Cai, Q. Li, G. Lu, H. S. Ryu, Y. Li, H. Jin, Z. Chen, Z. Tang, G. Lu, X. Hao, H. Y. Woo, C. Zhang, Y. Sun, *Nat. Commun.* **2022**, *13*, 2369.

[13] S. Liu, J. Yuan, W. Y. Deng, M. Luo, Y. Xie, Q. B. Liang, Y. P. Zou, Z. C. He, H. B. Wu, Y. Cao, *Nat. Photonics* **2020**, *14*, 300.

[14] H. Chen, R. Zhang, X. Chen, G. Zeng, L. Kobera, S. Abbrent, B. Zhang, W. Chen, G. Xu, J. Oh, S.-H. Kang, S. Chen, C. Yang, J. Brus, J. Hou, F. Gao, Y. Li, Y. F. Li, *Nat. Energy* **2021**, *6*, 1045.

[15] S. Few, J. M. Frost, J. Nelson, *Phys. Chem. Chem. Phys.* **2015**, *17*, 2311.

[16] W. G. Zhu, A. P. Spencer, S. Mukherjee, J. M. Alzola, V. K. Sangwan, S. H. Amsterdam, S. M. Swick, L. O. Jones, M. C. Heiber, A. A. Herzing, G. P. Li, C. L. Stern, D. M. DeLongchamp,

[17] O. Inganas, *Adv. Mater.* **2018**, *30*, 1800388.

[18] A. J. Heeger, *Adv. Mater.* **2014**, *26*, 10.

[19] Y. N. Zhang, Y. L. Xu, M. J. Ford, F. C. Li, J. X. Sun, X. F. Ling, Y. J. Wang, J. N. Gu, J. Y. Yuan, W. L. Ma, *Adv. Energy Mater.* **2018**, *8*, 1800029.

[20] S. Chandrabose, K. Chen, A. J. Barker, J. J. Sutton, S. K. K. Prasad, J. S. Zhu, J. D. Zhou, K. C. Gordon, Z. Q. Xie, X. W. Zhan, J. M. Hodgkiss, *J. Am. Chem. Soc.* **2019**, *141*, 6922.

[21] A. Baumann, T. J. Savenije, D. H. K. Murthy, M. Heeney, V. Dyakonov, C. Deibel, *Adv. Funct. Mater.* **2011**, *21*, 1687.

[22] M. Zhang, H. Wang, H. Tian, Y. Geng, C. W. Tang, *Adv. Mater.* **2011**, *23*, 4960.

[23] K. Ding, X. Liu, S. R. Forrest, *Nano Lett.* **2018**, *18*, 3180.

[24] D. Spoltore, A. Hofacker, J. Benduhn, S. Ullbrich, M. Nyman, O. Zeika, S. Schellhammer, Y. Fan, I. Ramirez, S. Barlow, M. Riede, S. R. Marder, F. Ortmann, K. Vandewal, *J. Phys. Chem. Lett.* **2018**, *9*, 5496.

[25] A. Melianas, V. Pranculis, D. Spoltore, J. Benduhn, O. Inganäs, V. Gulbinas, K. Vandewal, M. Kemerink, *Adv. Energy Mater.* **2017**, *7*, 1700888.

[26] T. Albes, L. Xu, J. Wang, J. W. P. Hsu, A. Gagliardi, *J. Phys. Chem. C* **2018**, *122*, 15140.

[27] O. J. Sandberg, S. Zeiske, N. Zarrabi, P. Meredith, A. Armin, *Phys. Rev. Lett.* **2020**, *124*, 128001.

[28] N. Yao, J. Wang, Z. Chen, Q. Bian, Y. Xia, R. Zhang, J. Zhang, L. Qin, H. Zhu, Y. Zhang, F. Zhang, *J. Phys. Chem. Lett.* **2021**, *12*, 5039.

[29] C. Xiao, C. Li, F. Liu, L. Zhang, W. Li, *J. Mater. Chem. C* **2020**, *8*, 5370.

[30] L. Zhu, J. Zhang, Y. Guo, C. Yang, Y. Yi, Z. Wei, *Angew. Chem., Int. Ed.* **2021**, *60*, 15348.

[31] M. B. Price, P. A. Hume, A. Ilina, I. Wagner, R. R. Tamming, K. E. Thorn, W. Jiao, A. Goldingay, P. J. Conaghan, G. Lakhwani, N. J. L. K. Davis, Y. F. Wang, P. Y. Xue, H. Lu, K. Chen, X. W. Zhan, J. M. Hodgkiss, *Nat. Commun.* **2022**, *13*, 2827.

[32] S. Karuthedath, J. Gorenflot, Y. Firdaus, N. Chaturvedi, C. S. P. De Castro, G. T. Harrison, J. I. Khan, A. Markina, A. H. Balawi, T. A. D. Peña, W. Liu, R.-Z. Liang, A. Sharma, S. H. K. Paleti, W. Zhang, Y. Lin, E. Alarousu, S. Lopatin, D. H. Anjum, P. M. Beaujuge, S. De Wolf, I. McCulloch, T. D. Anthopoulos, D. Baran, D. Andrienko, F. Laquai, *Nat. Mater.* **2021**, *20*, 378.

[33] S. R. Cowan, A. Roy, A. J. Heeger, *Phys. Rev. B* **2010**, *82*, 245207.

[34] L. J. A. Koster, V. D. Mihailetchi, R. Ramaker, P. W. M. Blom, *Appl. Phys. Lett.* **2005**, *86*, 123509.

[35] G. G. Malliaras, J. R. Salem, P. J. Brock, C. Scott, *Phys. Rev. B* **1998**, *58*, R13411.

[36] M. Osaka, D. Mori, H. Benten, H. Ogawa, H. Ohkita, S. Ito, *ACS Appl. Mater. Interfaces* **2017**, *9*, 15615.

[37] Y. Wu, S. Schneider, C. Walter, A. H. Chowdhury, B. Bahrami, H.-C. Wu, Q. Qiao, M. F. Toney, Z. Bao, *J. Am. Chem. Soc.* **2020**, *142*, 392.

[38] K. Vandewal, K. Tvingstedt, A. Gadisa, O. Inganäs, J. V. Manca, *Nat. Mater.* **2009**, *8*, 904.

[39] H. Q. Liu, M. Y. Li, H. B. Wu, J. Wang, Z. F. Ma, Z. Tang, *J. Mater. Chem. A* **2021**, *9*, 19770.

[40] K. Vandewal, J. Benduhn, V. C. Nikolis, *Sustainable Energy Fuels* **2018**, *2*, 538.

[41] K. Vandewal, K. Tvingstedt, A. Gadisa, O. Inganäs, J. V. Manca, *Phys. Rev. B* **2010**, *81*, 125204.

[42] S. Gelinas, A. Rao, A. Kumar, S. L. Smith, A. W. Chin, J. Clark, T. S. van der Poll, G. C. Bazan, R. H. Friend, *Science* **2014**, *343*, 512.

[43] R. Wang, C. F. Zhang, Q. Li, Z. G. Zhang, X. Y. Wang, M. Xiao, *J. Am. Chem. Soc.* **2020**, *142*, 12751.

[44] Y. Cho, T. Kumari, S. Jeong, S. M. Lee, M. Jeong, B. Lee, J. Oh, Y. D. Zhang, B. Huang, L. Chen, C. Yang, *Nano Energy* **2020**, *75*, 104896.

[45] O. Dyck, S. Hu, S. Das, J. Keum, K. Xiao, B. Khomami, G. Duscher, *Polymers* **2015**, *7*, 2446.

[46] J. R. Lakowicz, *Principles of Fluorescence Spectroscopy*, Springer, Boston MA, USA **2006**, https://doi.org/10.1007/978-0-387-46312-4.

[47] Y. Firdaus, V. M. Le Corre, S. Karuthedath, W. L. Liu, A. Markina, W. T. Huang, S. Chattopadhyay, M. M. Nahid, M. I. Nugraha, Y. B. Lin, A. Seitkhan, A. Basu, W. M. Zhang, I. McCulloch, H. Ade, J. Labram, F. Laquai, D. Andrienko, L. J. A. Koster, T. D. Anthopoulos, *Nat. Commun.* **2020**, *11*, 5220.

[48] H. Zhao, H. B. Naveed, B. J. Lin, X. B. Zhou, J. Yuan, K. Zhou, H. B. Wu, R. J. Guo, M. A. Scheel, A. Chumakov, S. V. Roth, Z. Tang, P. Muller-Buschbaum, W. Ma, *Adv. Mater.* **2020**, *32*, 2002302.

[49] A. Hexemer, W. Bras, J. Glossinger, E. Schaible, E. Gann, R. Kirian, A. MacDowell, M. Church, B. Rude, H. Padmore, *J. Phys.: Conf. Ser.* **2010**, *247*, 012007.

[50] E. Gann, A. T. Young, B. A. Collins, H. Yan, J. Nasiatka, H. A. Padmore, H. Ade, A. Hexemer, C. Wang, *Rev. Sci. Instrum.* **2012**, *83*, 045110.

[51] J. Yuan, D. Liu, H. Zhao, B. Lin, X. Zhou, H. B. Naveed, C. Zhao, K. Zhou, Z. Tang, F. Chen, W. Ma, *Adv. Energy Mater.* **2021**, *11*, 2100098.

[52] X. Li, Q. Zhang, J. Yu, Y. Xu, R. Zhang, C. Wang, H. Zhang, S. Fabiano, X. Liu, J. Hou, F. Gao, M. Fahlman, *Nat. Commun.* **2022**, *13*, 2046.

[53] C. Poelking, D. Andrienko, *J. Am. Chem. Soc.* **2015**, *137*, 6320.

[54] C. Poelking, M. Tietze, C. Elschner, S. Olthof, D. Hertel, B. Baumeier, F. Wurthner, K. Meerholz, K. Leo, D. Andrienko, *Nat. Mater.* **2015**, *14*, 434.